Published in final edited form as:
Neuroscience. 2008 May 15; 153(3): 654–663.

Physiology and morphology of callosal projection neurons in mouse

Raddy L. Ramos, **Danny M. Tam**, and **Joshua C. Brumberg***
Department of Psychology, Queens College, CUNY, Flushing, NY 11367

Abstract

In the mammalian neocortex, the corpus callosum serves as the major source of interhemispheric communication, comprised of axons from callosal neurons located in supragranular (II/III) and infragranular (V/VI) layers. We sought to characterize the physiology and morphology of supragranular and infragranular callosal neurons in mice using retrograde tracers and whole-cell patch clamp recordings. Whole-cell patch clamp recordings were made from retrogradely labeled callosal neurons following unilateral injection of fluorescent latex microspheres in the contralateral sensory-motor cortex. Following recordings and biocytin dialysis, labeled neurons were reconstructed using computer-assisted camera lucida (Neurolucida) for morphological analyses. Whole-cell recordings revealed that callosal neurons in both supra- and infragranular layers display very similar intrinsic membrane properties and are characteristic regular-spiking neurons. Morphological features examined from biocytin filled reconstructions as well as retrogradely BDA labeled cells did not reveal any differences. Analysis of spontaneous postsynaptic potentials from callosal neurons did reveal several differences including average amplitude, frequency, and decay time. These findings suggest that callosal neurons in both supra- and infragranular layers have similar phenotypes though belong to different local, intracortical networks.

Keywords

Interhemispheric; cortical circuits; barrel cortex

INTRODUCTION

A characteristic feature of the mammalian neocortex is its organization of neuronal lamina, each with distinct connectivity and function (reviewed in Jones 1984; White 1989; DeFelipe et al. 2002). Excitatory neurons with characteristic pyramidal cell morphologies and spiny dendrites comprise the majority of neurons in neocortex and are the principal cell-type arranged in discrete layers (Bayer and Altman, 1991; DeFelipe et al. 2002). Despite sharing gross morphological similarities, subpopulations of pyramidal neurons display different electrophysiological phenotypes, varying within and between lamina. For example, pyramidal neurons with different intrinsic electrophysiological properties have been observed within layer IV (Staiger et al. 2004), layer V (Kasper et al. 1994; Markram et al. 1997; Rumberger et al. 1998; Christophe et al. 2005; Le Be et al. 2007; Hattox and Nelson, 2007), as well as within

*Corresponding Author: Joshua C. Brumberg, PhD, Department of Psychology, Queens College, CUNY, Flushing, NY 11367, Email: joshua.brumberg@qc.cuny.edu, Phone: 718-997-3541, Fax: 718-997-3257.
SECTION EDITOR: **Cellular Neuroscience**: Dr. Menahem Segal, Weizmann Institute of Science, Department of Neurobiology, Hertzl Street, Rehovot 76100, Israel

layer VI (Brumberg et al. 2003; Yang et al. 1996) and include physiological phenotypes that generate burst discharges or regular spiking (Conners et al. 1982; McCormick et al. 1985).

Combined anatomical and physiological studies have revealed that pyramidal neurons with different physiological phenotypes often also display distinct morphologies and afferent/efferent projections. For example, burst-firing neurons in layer V of somatosensory cortex project to subcortical targets (tectum, brainstem, spinal cord) and have thick apical dendrites with large dendritic tufts that reach the pial surface (Kasper et al. 1994; Rumberger et al. 1998). In contrast, layer V neurons displaying a regular-spiking phenotype, lack subcortical projections and have thin apical dendrites with small-medium dendritic tufts (Kasper et al. 1994; Rumberger et al. 1998). More recently, these two populations of layer V neurons have been shown to preferentially form synaptic connections with neighboring neurons of a similar phenotype whereas connections between neurons of differing phenotypes were rarely observed (Markrum, 1997; Markrum et al. 1997; Le Be et al. 2007). These data demonstrate the presence of cortical networks composed of neurons with different morphology and physiology found within the same layer.

Neocortical circuits also include populations of pyramidal neurons that are found in different lamina but share similar projection targets. Such is the case with neurons that make inter-hemispheric projections via the corpus callosum. Primarily found in supragranular layers (II & III) as well as infragranular layers (V & VI), callosal neurons are thought to be the main anatomical substrate for information transfer between the cortical hemispheres as demonstrated by the dramatic sensation and perceptual deficits that are observed after callosal transaction (reviewed in Gazzaniga, 2006). The attenuation or elimination of epileptiform activity following callosal transaction also emphasizes the important role callosal neurons play in the spread of neural activity between the two hemispheres (reviewed in Reeves and O'Leary, 1985).

In the present report we examined whether callosal neurons found in supragranular layers share similar intrinsic electrophysiological properties with callosal neurons found in infragranular layers. Additionally, we utilized biocytin reconstructions in order to compare the dendritic morphology of callosal neurons found in supra- vs. infragranular layers. Our results provide important data on the intrinsic properties of callosal neurons and are relevant to models of information processing through micro and macro neocortical circuits.

EXPERIMENTAL PROCEDURES

Retrograde tracing of callosal neurons

In order to identify the distribution and morphology of callosal neurons, biotinylated dextran amine (BDA, 3000 MW; Molecular Probes) was injected into one hemisphere of CD1 mice of either sex as previously described (Rocco and Brumberg, 2007). Animals were anesthetized with a mixture of ketamine and xylazine and placed in a stereotaxic apparatus. After a small craniotomy was made, BDA (~1μL) was pressure injected via glass micropipettes or via a 10μL Hamilton Syringe.

Three days following injection, animals were perfused with 0.1M phosphate-buffered saline (PBS) followed by 4% paraformaldehyde in 0.1M PBS. Brains were removed and placed in the same fixative. Brains were blocked and 50 μm coronal sections were cut on a vibratome and sections collected in PBS. Biotin-avidin-HRP histochemistry was preformed in order to reveal BDA labeled neurons as previously described (Rocco and Brumberg, 2007). Sections were first placed in 1% H_2O_2/0.5% MEOH in PBS in order to quench endogenous peroxidase activity. After 3 washes in PBS, sections were permeabilized for one hour in PBS containing 0.2% Triton-X (Sigma). Sections were then placed in an avidin-HRP mixture (ABC Kit, Vector

Labs) overnight. Following 3 washes in PBS, sections were reacted in 0.05% diaminobenzidine/0.015% H_2O_2. Slices were washed in PBS, mounted onto gelatin coated-slides and coverslipped in DPX (Electron Microscopy Sciences).

Injection of rhodamine microspheres

To positively identify callosal neurons for whole-cell recordings, rhodamine-labeled latex microspheres (Lumafluor) were injected into one hemisphere on postnatal day (PND) 7–14 CD1 mice of either sex as described previously (Brumberg et al. 2003). Mice <P7 were anesthetized on ice while animals >P7 were anesthetized with ketamine and xylazine (intraperitoneal injection). After a small craniotomy was made, 0.5μL of beads was injected with a 10 μL Hamilton syringe. In some cases multiple injections were made. Mice were allowed to recover for a minimum of 3 days to ensure adequate retrograde transport to the opposite hemisphere.

Preparation of slices

Coronal slices of primary somatosensory cortex (300 μm thick) were prepared from P14-21, CD1 mice of either sex on a vibratome (VT1000S, Leica) in accordance with Queens College CUNY and National Institutes of Health guidelines for the use of laboratory animals and as described previously (Brumberg et al. 2003). Mice were anesthetized with an injection (0.1 ml ip) of a mixture of ketamine/xylazine. Following decapitation, the brain was quickly removed, blocked, and placed into ice-cold (4°C) oxygenated artificial cerebral spinal fluid (ACSF). ACSF contained (in mM) 125 NaCl, 2.5 KCl, 1 $MgCl_2$, 1.25 NaH_2PO_4, 2 $CaCl_2$, 25 $NaHCO_3$, and 25 d-glucose and was aerated with 95% O_2-5%CO_2 to a final pH of 7.4.

Electrophysiological recordings

Whole-cell recordings were made from retrogradely labeled callosal neurons. Neurons were visualized with IR-DIC and epifluorescent illumination (Olympus BX51WI). Patch pipettes (~4–7 MΩ tip resistance) were pulled on a Flaming/Brown microelectrode puller (P-97, Sutter Instruments). Pipettes were filled with (in mM) 120 KGlu, 10 NaCl, 20 KCl, 10 HEPES, 2 Mg-ATP, 0.3 Na-GTP, 0.5 EGTA, and 0.3–1% biocytin (wt/vol) for subsequent visualization of the neurons (see following text). Once a stable recording was obtained (resting V_m of <−55 mV, overshooting action potentials, ability to generate repetitive action potentials to a depolarizing current pulse), neurons were classified according to discharge pattern in response to a constant depolarizing current pulse (1000 ms) as intrinsically bursting, regular spiking, etc. (McCormick et al. 1985; Brumberg et al. 2000). Off-line analysis of action potential and passive membrane properties was performed using Clampfit9 (Molecular Devices). Statistics were computed using the SPSS software package (StatSoft). For between-group analyses, ANOVAs were conducted; post hoc two-tailed *t*-tests were used to determine the source of the variance, if any. Statistical significance was achieved when $p < 0.05$. All data are reported as means ± standard error of the mean (SEM) unless otherwise noted.

Spontaneous postsynaptic potentials (PSPs) were recorded at resting membrane potentials. These PSPs likely reflect inputs from putative excitatory neurons given the hyperpolarized membrane potentials of callosal neurons in our database of recordings. PSPs were isolated using a threshold detection algorithm (Clampfit9; Molecular Devices) in addition to post-hoc manual sorting. Using these methods, PSPs of ≥1mV were used in analyses. For determination of average instantaneous frequency of PSPs, both putative unitary and compound PSPs were included. For analyses of average amplitude, rise time, and decay time only manually-sorted, putative unitary PSPs were included.

Histology and Neuronal Reconstruction

Following recordings slices were placed in cold fixative (4% paraformaldehyde in 0.1 M phosphate buffer) and kept at 4°C for no more than 2 weeks. Biotin-avidin-HRP histochemistry was preformed as described above. Slices were not re-sectioned. For three-dimensional morphological reconstructions, the Neurolucida system (MicroBrightfield) was used in conjunction with an Olympus BX51 microscope using 4× (0.1 numerical aperture (NA)), 10× (0.4 NA) and 60× (1.4 NA, oil) objectives. Digital images were taken using an Optronics Microfire camera attached to a dedicated PC. Morphological measurements were made using the NeuroExplorer software package (MicroBrightfield). For Sholl analyses, 10 μm concentric circles were used beginning from the calculated center of mass of each reconstructed cell.

RESULTS

General morphology of supragranular and infragranular callosal neurons

We first set out to describe some general morphological features of callosal neurons in the mouse somatosensory cortex. As previously described in the rat (Wise and Jones, 1976; 1978) and more recently in mouse (Mitchell and Macklis, 2005), callosal neurons were found largely in homotopic regions opposite of the tracer injection site. Large tracer injections resulted in dozens-hundreds of labeled neurons per 50μm section, while small injections revealed 5–10 neurons per section. Regardless of the number of retrograde-labeled neurons observed, callosal neurons were always distributed in two horizontal bands composed of supragranular and infragranular layers and labeled neurons always demonstrated pyramidal morphologies. We did not observe any labeled neurons in layer I and few, if any, weakly-stained neurons were observed in layer IV (Ivy et al. 1984). Representative photomicrographs of retrograde-labeled callosal neurons in somatosensory cortex are found in Figure 1A, where the absence of labeled neurons in layer IV is clear, corresponding to areas of dense thalamocortical innervation (layer IV barrels; O'Leary et al. 1981; Mitchell and Macklis, 2005). Detailed morphological examination of callosal neurons was possible with BDA, which filled some secondary and few tertiary dendritic branches. As is shown in Figure 1B–C, callosal neurons found in supragranular layers had very homogeneous morphologies with apical dendrites which branched at the layer I/II border and with dendritic tufts that extended to the pial surface. Layer V callosal neurons also demonstrated pyramidal morphologies; however, the apical dendrites of these cells could not be followed superficial to layer IV (Figure 1D–E).

We quantified somatic and apical dendritic profiles of callosal neurons found in supragranular vs. infragranular layers using computer-assisted camera-lucida. For these analyses, the perimeter of labeled somata was traced and the length of the apical dendrite was measured from the base to the branch point at the site of the terminal dendritic tufts. Figure 1F contains a representative cumulative histogram of the calculated somata area (μm^2) of labeled supragranular callosal (SC; n = 165) and infragranular callosal (IC; n = 52) cells. SC neurons had somata areas measuring 105.94 ± 23.27 μm^2, while IC neurons that somata measuring 108.87 ± 22.15 μm^2; these data were not significantly different. As shown in Figure 1G, the perimeter of labeled somata also revealed no difference between SC cells (42.01 ± 20.67 μm) and IC cells (42.26 ± 19.66 μm). Finally, the length of apical dendrites of SC and IC cells was measured and revealed no significant difference (SC: 103.08 ± 13.29 μm; IC: 105.89 ± 14.06 μm). These data are consistent with the observation that IC cells had apical dendritic profiles which did not reach supragranular layers similar to that described previously in rat (Hubener and Bolz, 1988; Koester and O'Leary, 1992).

Physiological properties of callosal neurons in supra- and infragranular layers

We used fluorescent microspheres in order to label SC and IC neurons for targeted whole-cell recordings *in vitro*. Whole-cell patch-clamp recordings were obtained from 25 SC cells and 28

IC cells and a number of intrinsic membrane properties of these cells were examined (Table 1). Figure 2 contains IR-DIC (A) and epifluorescent (B) photomicrographs of a representative slice with retrogradely-labeled callosal neurons. Photomicrographs of a labeled SC neuron are shown in Figure 2B–C.

The resting membrane potential of neurons was determined soon after whole-cell configuration was achieved. As shown in Figure 2D, SC neurons exhibited a slightly more depolarized average resting membrane potential of −75.33±0.57 mV, while IC neurons exhibited a resting membrane potential of −73.44±0.72 mV. A one-way ANOVA revealed a significant difference between SC and IC resting membrane potentials ($p < 0.05$).

The input resistance of recorded neurons was calculated by the slope of a line fitted to the current vs. voltage relationship for hyperpolarizing currents steps of −25 to −200pA (25pA increments). Calculations were derived from peak voltage responses as well as the voltage measured 25ms before the offset of the current step. This was intended to reveal any time-dependent inward rectification (sag responses). As shown in Figure 2E, the average input resistance calculated from peak responses for SC neurons was 423.82±102.79 MΩ, whereas the average input resistance for IC neurons was 431.50±84.62 MΩ. A one-way ANOVA revealed no significant difference between the input resistance measured in SC and IC cells. Input resistance calculated from late voltage responses (25ms before the offset of the current step) were 367.07±71.99 MΩ for SC neurons and 377.94±91.66 MΩ for IC neurons. A one-way ANOVA revealed no significant difference. We next calculated the input resistance change observed as the difference between the resistance measured during the peak responses and that measured during late responses. This analysis revealed a decrease of 45.88±11.13 MΩ for SC neurons and 64.42±12.63 MΩ for IC neurons indicating moderate time dependent inward rectification from both cell types (Figure 2F). A one-way ANOVA revealed no significant difference.

A number of suprathreshold response properties were investigated in SC and IC cells in response to depolarizing current steps including action potential threshold, half-width, and rise time. As shown in Figure 2G, SC cells displayed an average action potential threshold of −40.93 ±0.51mV while IC cells displayed an average threshold of −41.25±0.38mV. These data were not significantly different. Average action potential width at half amplitude of SC cells (recordings done at ~22°C) was 2.45±0.1 ms compared to 2.21±0.07 ms which was observed for IC cells. A one-way ANOVA revealed a significant difference between action potential width measured in SC and IC cells ($p < 0.05$; Figure 2H). As shown in Figure 2I, action potential rise time was also measured and in SC (0.49±0.01 ms) and IC cells (0.49±0.02 ms). These data were not significantly different.

The number of action potentials elicited by suprathreshold current steps was measured in SC and IC cells. As shown in Figure 3A–B, both SC and IC cells exhibited increases in the number of spikes elicited by increasing current injection. Repeated measures ANOVA indicated that both cell-types displayed significant increases in action potential number with increasing current steps (SC cells: $p < 0.001$; IC cells: $p < 0.001$). Interestingly, as shown in Figure 3B, SC neurons displayed asymptotic levels of firing to current steps >250pA while IC cells continued to display increases in spike number. Repeated-measures ANOVA revealed a significant difference in the number of spikes elicited to increasing current steps between SC and IC cells (i.e. a significant interaction between *current injection* vs. *cell-type*; $p < 0.001$). We examined this difference further and performed independent samples t-tests on responses to each current step. These analyses revealed significantly greater firing displayed by IC cells, compared to SC cells, for current injections measuring (in pA) 275, 300, 400, 425, and 475 (all $p < 0.05$).

The maximum firing frequency recorded in SC and IC cells was compared in response to increasing current steps. For each cell, the maximum firing frequency was always observed at the beginning of each response (i.e. the first inter-spike interval that was recorded). As shown in Figure 3C, similar increases in the maximum firing rate were exhibited by both cell types. Maximum firing changed significantly with increasing current intensity (repeated measures ANOVA; $p < 0.001$) although no significant interaction was observed (*current intensity* vs. *celltype*). These data indicate that both SC and IC cells show similar changes in firing frequency in response to increasing depolarization.

Both SC and IC cells exhibited strong action potential frequency adaptation in response to suprathreshold current injection. We quantified the rate of adaptation by SC and IC cells in response to a 200pA current step (a current step which elicited the same numbers of action potentials and firing rates in both cell-types). Firing rates were normalized relative to that computed for the first inter-spike interval (ISI), which always displayed the maximum firing frequency. Each subsequent ISI was expressed as a ratio relative to the first ISI. As is shown in Figure 3D, both SC and IC cells displayed strong firing rate adaptation. Repeated measures ANOVA of firing rate adaptation measures between SC and IC cells revealed no significant differences. This signature response adaptation phenotype displayed by SC and IC cells is reminiscent of the regular-spiking type-2 (RS_2) pyramidal cells reported by Degenetais et al. (2002).

In summary, SC and IC neurons display similar intrinsic physiological properties and only subtle differences in resting membrane potential and action potential duration. Taken together the above results suggest that callosal projection neurons are a homogeneous cell class despite their differences in laminar position.

Analysis of Spontaneous Postsynaptic Potentials in Callosal Neurons

Despite sharing similar morphological and intrinsic physiological properties, SC and IC neurons may participate in different local, intracortical circuits. Therefore, we recorded spontaneous postsynaptic potentials (PSPs) in both SC and IC neurons as a measure of activity from presynaptic inputs (Figure 4A). Analysis of PSPs were recorded at resting membrane potentials in SC and IC neurons revealed higher frequency PSPs in SC neurons (in Hz: SC=22.13±1.17; IC=12.79±0.64; $p<0.001$) but larger amplitude PSPs in IC neurons (in pA: SC=2.86±0.08; IC=3.99±0.08; $p<0.001$). These data are shown in Figure 4B–C and suggest that local inputs onto SC neurons are more spontaneously active *in vitro* than those onto IC neurons. Interestingly, PSP rise times were not different between cell-types (in ms: SC=7.11 ±0.29; IC=5.64±0.20) but decay times were longer in IC neurons (in ms: SC=42.69±1.41; IC=50.58±0.77; $p<0.02$). These data are shown in Figure 4D–E.

Morphological reconstruction of physiologically-identified, callosal neurons in supra- and infragranular layers

Three-dimensional reconstructions of biocytin-filled neurons were used in order to determine more detailed morphological characteristics of physiologically-identified SC (n=21) and IC (n=15) cells. Similar to our morphological analyses on BDA-labeled neurons (Figure 1), all reconstructed neurons had pyramidal morphologies. Unlike observed with BDA, biocytin labeled numerous fine-caliber branches on distal dendrites and in some cases dendritic spines were also evident. Figure 5A illustrates representative examples of reconstructed SC and IC neurons. We observed significant differences in the somatic area and perimeter measurements between SC and IC neurons (independent samples t-test; both $p < 0.02$). Reconstructed IC neurons had slightly larger somatic perimeters (50.03 ± 1.68μm) and areas (162.76 ± 10.31μm) compared to SC cells (perimeter: 45.07 ± 1.13μm; area: 127.97 ± 8.08μm). These

results differ from our measurements from BDA-labeled somata but may reflect the smaller sample size of biocytin reconstructed neurons.

Qualitatively, SC neurons appeared to have more numerous and elaborate dendritic processes. For example, there was a trend for SC neurons to have more dendritic nodes (branches) on apical dendrites (5.57 ± 0.712) as well as greater total dendritic length of apical dendrites (712.6 ± 75.46μm) compared to IC cells (apical nodes: 3.8 ± 0.51; total apical length: 516.34 ± 69.19). However, quantitative analyses of numerous measures of dendritic morphology of apical as well as basal dendrites did not reveal any significant differences (independent samples t-test; all $p > 0.05$). We further examined the distribution and morphology of SC and IC dendrites with Sholl analysis, which reveals the spatial location of dendrites and their branching patterns relative to the soma. As shown in Figure 5B Sholl analyses revealed no differences between groups for measures of dendritic intersections and dendritic length. These data suggest that both SC and IC neurons share largely similar morphologies despite residing in different lamina. Furthermore, our results are similar to previous analyses of IC neurons in rats (Le Be et al. 2007)

DISCUSSION

Complex cognitive function emerges from the diversity of neocortical neurons and the dynamic properties of their synaptic connections. Among a growing list of schemes used to describe cortical neurons, classification according to afferent projection target is useful and has been previously used to distinguish among neurons found in individual layers. For example, neurons within layer V can be distinguished by their projection target which also correlates with morphological differences as well as intrinsic physiological properties (Kasper et al. 1994; Rumberger et al. 1998) and responses to peripheral stimulation (Swadlow, 1989; 1990). More recently, a number of molecular markers have been found which distinguish among different layer V neurons (Hevner et al. 2003; Molnar and Cheung, 2006; Nelson et al. 2006a b; Sugino et al. 2006) suggesting complementary genetic origins of morphological, physiological, and connectivity differences between neurons within the same lamina.

In the present experiment we compared neurons found in different neocortical lamina that share similar interhemispheric projection patterns. Callosal neurons were retrogradely labeled with BDA in order to describe their spatial/areal position as well as some morphological features. These analyses revealed that callosal neurons are preferentially found in two discrete bands in supragranular (II/III) and infragranular layers (V/VI). Using BDA we observed that all labeled neurons have characteristic pyramidal cell morphologies indicative of putative glutamatergic neurons. These data contrast recent reports of a small population of retrogradely-labeled neurons which co-localize GABAergic markers (1–5% of callosal neurons; Gonchar et al. 1994; Fabri and Manzoni, 2004). Differences in the species (mouse vs. rat/cat) and tracers (BDA vs. WGA, cholera toxin β-subunit) used between theses studies may underlie these different results.

Unlike layer V-corticofugal neurons (Kasper et al. 1994; Rumberger et al. 1998; Le Be et al. 2007; Christophe et al. 2005) that have thick tufted apical dendrites that extend to the pial surface callosal neurons in layer V have substantially shorter and thinner apical dendrites. Recent Sholl analysis of these two layer V neuron populations in rats, revealed apical dendrites in callosal neurons which were more than 200μm shorter than the thick tufted layer V neurons (Le be et al. 2007). Our analysis of IC neurons in mouse also revealed apical dendrites which do not extend past layer IV. Moreover, the apical dendritic length of IC neurons was found to be no different from that observed in SC neurons, all of which have apical dendrites that do reach the pial surface. Together with measures of somata area and perimeter which were not different between BDA-labeled SC and IC neurons, these data point to general morphological

similarities among callosal neurons found in different lamina. Our results in mice are consistent with studies conducted in rats demonstrating short apical dendrites on IC neurons revealed by retrograde tracing with lipophilic dyes (Hubener and Bolz, 1988; Koester and O'Leary, 1992) as well as following reconstruction of biocytin-filled neurons (Kasper et al. 1994; Le Be et al. 2007).

We used whole-cell patch recordings in order to describe a number of intrinsic membrane properties of SC and IC neurons. Surprisingly few differences were found in the resting and active properties measured, indicating that these cells-types likely share a similar complement of resting and active ion channels. Both SC and IC cells exhibited a 'regular-spiking' phenotype with rapidly-adapting action potentials. The 'regular-spiking' phenotype displayed by SC and IC neurons likely has implications for the types of synaptic inputs that can be encoded temporally by these cells (Brumberg, 2002). These data are in contrast to the high frequency firing regimes displayed GABAergic 'fast-spiking' neurons (Connors et al. 1982; McCormick et al. 1985; Descalzo et al. 2005) as well as layer V 'burst-firing' corticotectal neurons (Kasper et al. 1994; Rumberger et al. 1998; Christophe et al 2005; Le Be et al. 2007). Rapid action potential adaptation by SC and IC neurons also indicates limited ability to encode long duration inputs unlike 'fast-spiking' neurons that can maintain high frequency firing for prolonged periods (McCormick et al. 1985; Descalzo et al. 2005).

Interestingly, despite similar intrinsic physiological properties, we observed differences in the average frequency and amplitude of PSPs recorded in SC and IC neurons. While the exact presynaptic elements responsible for the PSPs we recorded are unknown, our data suggest that those neurons contacting SC cells remain more active *in vitro* resulting in the observation of more frequent PSPs in SC neurons. One important clue as to the presynaptic elements of intracortical circuits of IC neurons was recently provided by Le Be at el. (2007). Using paired recordings, these authors found only ~3% probability of 2 IC neurons showing synaptic connectivity, suggesting that IC neurons form circuits with diverse, non-callosal projecting neurons.

It is not known where on the dendritic tree the synaptic contacts responsible for the PSPs recorded in callosal neurons are located. Our results revealing larger amplitude PSPs in IC neurons may indicate that synapses are found more proximal to the soma (the site where recordings were made). Alternatively, a number of postsynaptic mechanisms would result in higher amplitude PSPs in IC neurons including greater numbers or different classes of postsynaptic receptors. The observation that PSPs in IC neurons had slower decay times than in SC neurons is perhaps indicative of postsynaptic receptor differences (Mainen et al. 1996, Spruston et al. 1999).

Following recording and biocytin dialysis, the morphology of SC and IC neurons were reconstructed and more dendritic characteristics were examined. These data revealed greater morphological detail than observed with BDA, which was due to filling of secondary, tertiary, and higher-order dendritic branches with biocytin. Surprisingly, quantitative measures of apical and basal dendritic branching and length did not reveal any significant differences. Together with a lack of observed differences following Sholl analyses, these data point to morphological similarities among SC and IC neurons.

The potential for incomplete biocytin dialysis during whole-cell recordings as well as disruption of neuronal morphology due to the slicing procedure are important caveats when interpreting our morphological results from *in vitro* slices. While these factors generally exaggerate differences between neuronal groups, these factors might also have contributed to our inability to find larger morphometric differences between SC and IC neurons. Nevertheless, dramatic physiologic differences have been previously observed in neurons with strikingly

similar morphologies (Golding et al. 2001). Conversely, dramatic morphological differences are found in neurons with similar intrinsic membrane properties (Staiger et al. 2004; Schubert et al. 2006). Our results point to similarities of both physiology and morphology of callosal neurons.

Unlike SC neurons, we did not observe any IC neurons with apical dendrites which extended to the pial surface. In light of the fact that similar results were observed with biocytin dialysis or retrograde transport of BDA, short apical dendrites may indeed be a characteristic feature of IC neurons despite our limited sampling techniques. This is consistent with the finding that IC neurons in rat (Hubener and Bolz, 1988; Koester and O'Leary, 1992; Le Be et al. 2007) as well as monkey (Soloway et al. 2002) neocortex also exhibit short apical dendrites. However, recent biocytin reconstruction of layer V callosal neurons in C57BL/6J inbred mice revealed neurons with apical dendrites that reached the pial surface with narrow dendritic tufts (Hattox and Nelson, 2007). Why the morphology of callosal neurons in C57BL/6J differs from outbred mice (used in the present study), rats, and monkeys is not known.

Callosal neurons and cortical function

The precise role of the callosal activity in shaping cortical function remains unknown. Found in both supragranular and infragranular layers, callosal neurons are likely activated by both intracortical as well as subcortical inputs, suggesting that ongoing callosal activity is a general feature cortical processing (Wiest et al. 2005). Consistent with this hypothesis, unilateral lesion of the rodent somatosensory cortex results in a dramatic decrease in spontaneous activity of contralateral pyramidal cells found throughout the depth of cortex (Rema and Ebner, 2003). Evoked responses to peripheral stimulation (whisker deflections) are also reduced above, below, and within layer IV after contralateral lesion (Rema and Ebner, 2003; Li et al 2005). Thus, callosal neurons serve as a source of tonic excitation with the ability to modulate thalamocortical inputs.

Stimulation of callosal fibers results in excitation of both pyramidal neurons as well as interneurons of the contralateral hemisphere (Cisse et al. 2003; Karayannis et al. 2006; Petreanu et al. 2007). Therefore, callosal neurons also form part of an interhemispheric feed-forward inhibitory circuit which may serve to limit the amplitude and duration of callosal excitation. Nevertheless, the net result of callosal activity is strong excitation of contralateral targets. Not surprisingly, repetitive electrical stimulation of callosal fibers can result in epileptiform activity *in vivo* (Cisse et al 2004). Likewise, epileptiform activity is attenuated or eliminated following callosal transaction (reviewed in Reeves and O'Leary, 1985).

Callosal neurons in supragranular and infragranular layers constitute a homogeneous neuronal population as assessed by our physiological and morphological methods. However, SC and IC neurons might still participate in different cortical networks as was revealed by analysis of spontaneous PSPs of SC and IC neurons. For instance, intracortical or subcortical afferents that preferentially target supragranular layers could exclusively activate SC neurons and not IC neurons given our observation that IC neurons have apical dendrites that do not extent past layer IV. Candidate subcortical inputs preferentially targeting SC neurons include afferents from non-specific thalamic nuclei which target layer I (Galazo et al. in press). Conversely, cortical afferents preferentially targeting infragranular layers could exclusively activate IC and not SC neurons.

Acknowledgements

We thank Mary Rocco and Aileen Tlamsa for assistance with BDA injections. RLR was supported by the Howard Hughes Medical Institute (Undergraduate Science Education Program to Queens College, CUNY #52005118). PSC-CUNY, CUNY-Equipment Grants, and NS058758-01A1 to JCB.

Abbreviations

ACSF
artificial cerebral spinal fluid

ANOVA
analysis of variance

BDA
biotinylated dextran amine

IC
infragranular callosal neurons

IR-DIC
infrared differential interference contrast

ISI
inter-spike interval

HRP
horseradish peroxidase

PBS
phosphate-buffered saline

SC
supragranular callosal neurons

References

Brumberg JC. Firing pattern modulation by oscillatory input in supragranular pyramidal neurons. Neuroscience 2002;114(1):239–46. [PubMed: 12207969]

Brumberg JC, Nowak LG, McCormick DA. Ionic mechanisms underlying repetitive high frequency burst firing in cortical neurons. J Neurosci 2000;20:4829–4843. [PubMed: 10864940]

Brumberg JC, Hamzei-Sichani F, Yuste R. Morphological and Physiological Characterization of Layer VI Corticofugal Neurons of Mouse Primary Visual Cortex. J Neurophysiol 2003;89(5):2854–2867. [PubMed: 12740416]

Christophe E, Doerflinger N, Lavery DJ, Molnar Z, Charpak S, Audinat E. Two populations of layer V pyramidal cells of the mouse neocortex: development and sensitivity to anesthetics. J Neurophysiol 2005;94(5):3357–67. [PubMed: 16000529]

Cisse Y, Crochet S, Timofeev I, Steriade M. Synaptic responsiveness of neocortical neurons to callosal volleys during paroxysmal depolarizing shifts. Neuroscience 2004;124(1):231–9. [PubMed: 14960354]

Cisse Y, Grenier F, Timofeev I, Steriade M. Electrophysiological properties and input-output organization of callosal neurons in cat association cortex. J Neurophysiol 2003;89(3):1402–13. [PubMed: 12626619]

Connors BW, Gutnick MJ, Prince DA. Electrophysiological properties of neocortical neurons in vitro. J Neurophysiol 1982;48(6):1302–20. [PubMed: 6296328]

Degenetais E, Thierry AM, Glowinski J, Gioanni Y. Electrophysiological properties of pyramidal neurons in the rat prefrontal cortex: an in vivo intracellular recording study. Cereb Cortex 2002;12(1):1–16. [PubMed: 11734528]

Descalzo VF, Nowak LG, Brumberg JC, McCormick DA, Sanchez-Vives MV. Slow adaptation in fast-spiking neurons of visual cortex. J Neurophysiol 2005;93(2):1111–8. [PubMed: 15385594]

Fabri M, Manzoni T. Glutamic acid decarboxylase immunoreactivity in callosal projecting neurons of cat and rat somatic sensory areas. Neuroscience 2004;123(2):557–66. [PubMed: 14698762]

Gazaniga MS. Forty-five years of split-brain research and still going strong. Nat Rev Neurosci 2005;6 (8):653–9. [PubMed: 16062172]

Galazo MJ, Martinez-Cerdeno V, Porrero C, Clasca F. Embryonic and Postnatal Development of the Layer I-Directed ("Matrix") Thalamocortical System in the Rat. Cereb Cortex. 2007 May 20, 2007;10.1093/cercor/bhm059

Golding NL, Kath WL, Spruston N. Dichotomy of action-potential backpropagation in CA1 pyramidal neuron dendrites. J Neurophysiol 2001;86(6):2998–3010. [PubMed: 11731556]

Gonchar YA, Johnson PB, Weinberg RJ. GABA-immunopositive neurons in rat neocortex with contralateral projections to S-I. Brain Res 1995;697(1–2):27–34. [PubMed: 8593589]

Hattox AM, Nelson SB. Layer V neurons in mouse cortex projecting to different targets have distinct physiological properties. J Neurophysiol 2007;98(6):3330–40. [PubMed: 17898147]

Hevner RF, Daza RA, Rubenstein JL, Stunnenberg H, Olavarria JF, Englund C. Beyond laminar fate: toward a molecular classification of cortical projection/pyramidal neurons. Dev Neurosci 2003;25 (2–4):139–51. [PubMed: 12966212]

Hubener M, Bolz J. Morphology of identified projection neurons in layer 5 of rat visual cortex. Neurosci Lett 1988;94(1–2):76–81. [PubMed: 2468117]

Ivy GO, Gould HJ 3rd, Killackey HP. Variability in the distribution of callosal projection neurons in the adult rat parietal cortex. Brain Res 1984;306(1–2):53–61. [PubMed: 6205722]

Jones, EG. Laminar distribution of cortical efferent cells. In: Peters, A.; Jones, EG., editors. Cerebral Cortex, Cellular Components of the Cerebral Cortex. 1. New York: Plenum; 1984. p. 521-553.

Kang Y, Kayano F. Electrophysiological and morphological characteristics of layer VI pyramidal cel s in the cat motor cortex. J Neurophysiol 1994;72:578–591. [PubMed: 7983520]

Karayannis T, Huerta-Ocampo I, Capogna M. GABAergic and pyramidal neurons of deep cortical layers directly receive and differently integrate callosal input. Cereb Cortex 2007;17(5):1213–26. [PubMed: 16829551]

Kasper EM, Larkman AU, Lubke J, Blakemore C. Pyramidal neurons in layer 5 of the rat visual cortex. I. Correlation among cell morphology, intrinsic electrophysiological properties, and axon targets. J Comp Neurol 1994;339(4):459–74. [PubMed: 8144741]

Koester SE, O'Leary DD. Functional classes of cortical projection neurons develop dendritic distinctions by class-specific sculpting of an early common pattern. J Neurosci 1992;12(4):1382–93. [PubMed: 1556599]

Kumar SS, Huguenard JR. Pathway-specific differences in subunit composition of synaptic NMDA receptors on pyramidal neurons in neocortex. J Neurosci 2003;23(31):10074–83. [PubMed: 14602822]

Kumar SS, Huguenard JR. Properties of excitatory synaptic connections mediated by the corpus callosum in the developing rat neocortex. J Neurophysiol 2001;86(6):2973–85. [PubMed: 11731554]

Le Be JV, Silberberg G, Wang Y, Markram H. Morphological, Electrophysiological, and Synaptic Properties of Corticocallosal Pyramidal Cells in the Neonatal Rat Neocortex. Cereb Cortex 2007;17 (9):2204–13. [PubMed: 17124287]

Li L, Rema V, Ebner FF. Chronic suppression of activity in barrel field cortex downregulates sensory responses in contralateral barrel field cortex. J Neurophysiol 2005;94(5):3342–56. [PubMed: 16014795]

Mainen ZF, Carnevale NT, Zador AM, Claiborne BJ, Brown TH. Electrotonic architecture of hippocampal CA1 pyramidal neurons based on three-dimensional reconstructions. J Neurophysiol 1996;76(3):1904–23. [PubMed: 8890303]

Markram H. A network of tufted layer 5 pyramidal neurons. Cereb Cortex 1997;7(6):523–33. [PubMed: 9276177]

Markram H, Lubke J, Frotscher M, Roth A, Sakmann B. Physiology and anatomy of synaptic connections between thick tufted pyramidal neurones in the developing rat neocortex. J Physiol 1997;500(Pt 2): 409–40. [PubMed: 9147328]

McCormick DA, Connors BW, Lighthall JW, Prince DA. Comparative electrophysiology of pyramidal and sparsely spiny stellate neurons of the neocortex. J Neurophysiol 1985;54:782–806. [PubMed: 2999347]

Mitchell BD, Macklis JD. Large-scale maintenance of dual projections by callosal and frontal cortical projection neurons in adult mice. J Comp Neurol 2005;482(1):17–32. [PubMed: 15612019]

Molnar Z, Cheung AF. Towards the classification of subpopulations of layer V pyramidal projection neurons. Neurosci Res 2006;55(2):105–15. [PubMed: 16542744]

Nelson SB, Hempel C, Sugino K. Probing the transcriptome of neuronal cell types. Curr Opin Neurobiol 2006;16(5):571–6. [PubMed: 16962313]

Nelson SB, Sugino K, Hempel CM. The problem of neuronal cell types: a physiological genomics approach. Trends Neurosci 2006;29(6):339–45. [PubMed: 16714064]

O'Leary DD, Stanfield BB, Cowan WM. Evidence that the early postnatal restriction of the cells of origin of the callosal projection is due to the elimination of axonal collaterals rather than to the death of neurons. Brain Res 1981;227(4):607–17. [PubMed: 7260661]

Petreanu L, Huber D, Sobczyk A, Svoboda K. Channelrhodopsin-2-assisted circuit mapping of long-range callosal projections. Nat Neurosci 2007;10(5):663–8. [PubMed: 17435752]

Reeves, A.; O'Leary, P. Total corpus callosotomy for control of medically intractable epilepsy. In: Reeves, A., editor. Epilepsy and the Corpus Callosum. New York: Plenum Press; 1985. p. 269-280.

Rema V, Ebner FF. Lesions of mature barrel field cortex interfere with sensory processing and plasticity in connected areas of the contralateral hemisphere. J Neurosci 2003;23(32):10378–87. [PubMed: 14614097]

Rocco MM, Brumberg JC. The sensorimotor slice. J Neurosci Methods 2007;162(1–2):139–47. [PubMed: 17307257]

Rumberger A, Schmidt M, Lohmann H, Hoffmann KP. Correlation of electrophysiology, morphology, and functions in corticotectal and corticopretectal projection neurons in rat visual cortex. Exp Brain Res 1998;119(3):375–90. [PubMed: 9551838]

Schubert D, Kotter R, Luhmann HJ, Staiger JF. Morphology, electrophysiology and functional input connectivity of pyramidal neurons characterizes a genuine layer Va in the primary somatosensory cortex. Cereb Cortex 2006;16(2):223–36. [PubMed: 15872153]

Soloway AS, Pucak ML, Melchitzky DS, Lewis DA. Dendritic morphology of callosal and ipsilateral projection neurons in monkey prefrontal cortex. Neuroscience 2002;109(3):461–71. [PubMed: 11823059]

Spruston, N.; Stuart, G.; Hausser, M. Dendritic integration. In: Stuart, G.; Spruston, N.; Hausser, M., editors. Dendrites. Oxford: Oxford University Press; 1999. p. 231-270.

Staiger JF, Flagmeyer I, Schubert D, Zilles K, Kotter R, Luhmann HJ. Functional diversity of layer IV spiny neurons in rat somatosensory cortex: quantitative morphology of electrophysiologically characterized and biocytin labeled cells. Cereb Cortex 2004;14(6):690–701. [PubMed: 15054049]

Sugino K, Hempel CM, Miller MN, Hattox AM, Shapiro P, Wu C, Huang ZJ, Nelson SB. Molecular taxonomy of major neuronal classes in the adult mouse forebrain. Nat Neurosci 2006;9(1):99–107. [PubMed: 16369481]

Swadlow H. Efferent neurons and suspected interneurons in S-1 vibrissa cortex of the awake rabbit: receptive fields and axonal properties. J Neurophysiol 1989;62(1):288–308. [PubMed: 2754479]

Swadlow H. Efferent neurons and suspected interneurons in S-1 forelimb representation of the awake rabbit: receptive fields and axonal properties. J Neurophysiol 1990;63(6):1477–98. [PubMed: 2358887]

Yang CR, Seamens JK, Gorelova N. Electrophysiological and morphological properties of layers V-VI principal pyramidal cells in rat prefrontal cortex in vitro. J Neurosci 1996;16:1904–1921. [PubMed: 8774458]

Wiest MC, Bentley N, Nicolelis MAL. Heterogeneous integration of bilateral whisker signals by neurons in primary somatosensory cortex of awake rats. J Neurophysiol 2005;93:2966–2973. [PubMed: 15563555]

White, EL. Cortical Circuits, Synaptic Organization of the Cerebral Cortex, Structure, Function, and Theory. Boston, MA: Birkhauser; 1989.

Wise SP, Jones EG. The organization and postnatal development of the commissural projection of the rat somatic sensory cortex. J Comp Neurol 1976;168(3):313–43. [PubMed: 950383]

Wise SP, Jones EG. Developmental studies of thalamocortical and commissural connections in the rat somatic sensory cortex. J Comp Neurol 1978;178(2):187–208. [PubMed: 627623]

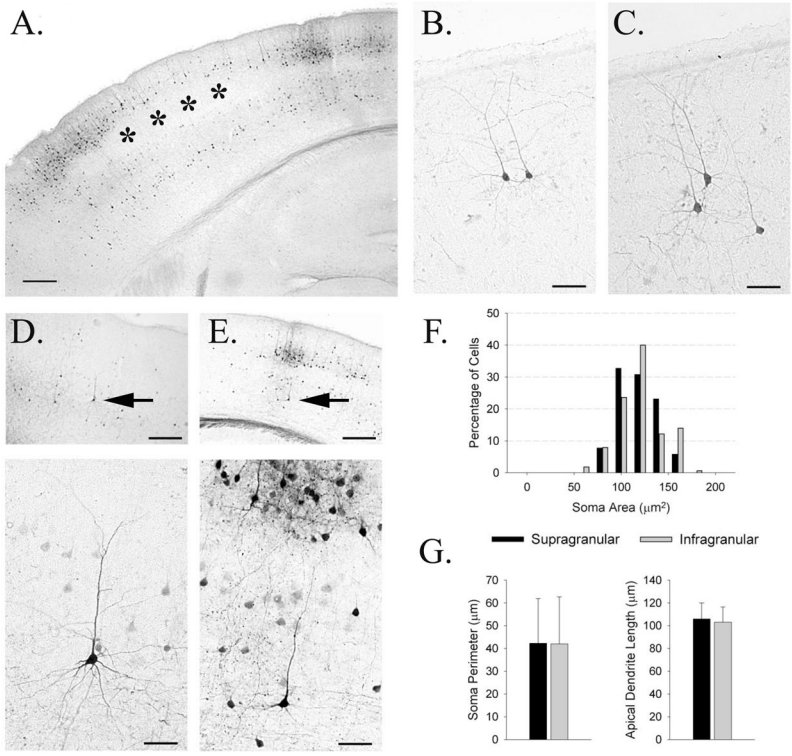

Figure 1.

Retrograde tracing of callosal neurons with BDA. A. Low-power photomicrograph of labeled callosal neurons in somatosensory cortex. Note two horizontal bands labeled cells in supragranular and infragranular layers and absence of cells in layer IV Barrels (asterisks). B–C. Photomicrographs of representative supragranular callosal neurons with characteristic pyramidal morphologies. D–E. Photomicrographs of representative infragranular callosal neurons. Top panels show location of cells within the depth of cortex (arrows); bottom panels illustrate the short apical dendritic lengths. F–G. Quantification of somatic profiles and apical dendritic lengths. Calibration: A. upper panels of D–E = 250μm; B–C. lower panels of D–E. = 50μm.

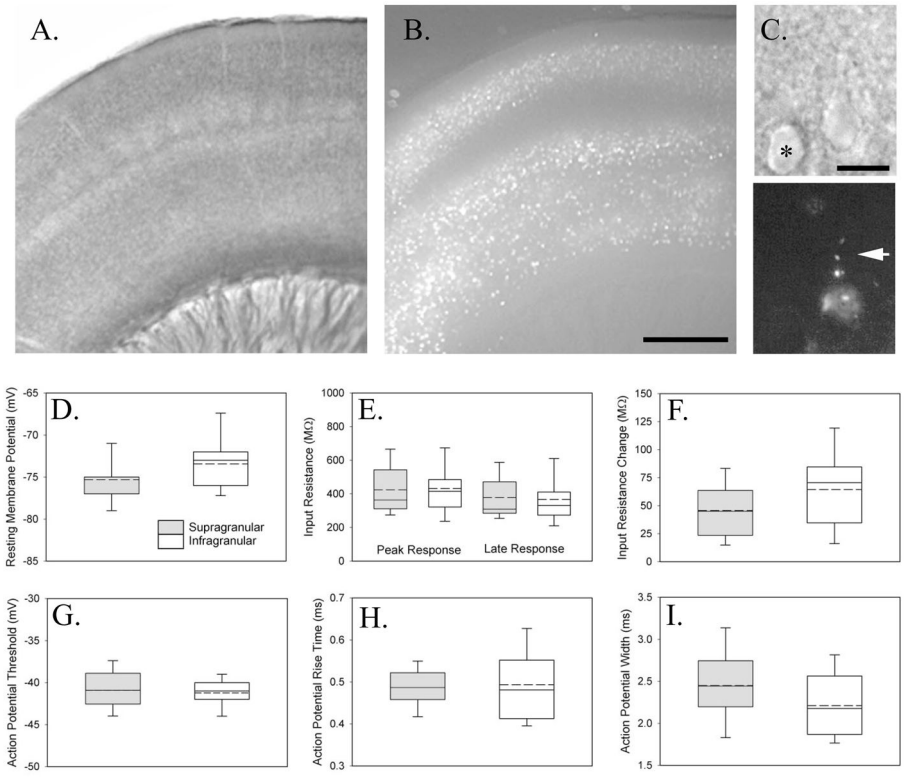

Figure 2.

Retrograde tracing of identified callosal neurons for whole-cell recording. A., IR-DIC photomicrograph of labeled slice maintained *in vitro*. B. Epifluorescent micrograph of same slice as in A, demonstrating labeled callosal neurons. Note lack of labeling in layer IV. C. IR-DIC (top) and epifluorescent micrograph of a labeled supragranular neuron. Note unlabeled neuron (asterisk) and apical dendrite of labeled neuron (arrow). D–I. Measures of passive and active properties of callosal neurons. The boundary of the box closest to zero indicates the 25th percentile while the boundary of the box farthest from zero indicates the 75th percentile. Solid line within the box marks the median while a dashed line marks the mean. Error bars above and below the box indicate the 90th and 10th percentiles. Calibration in A–B: 500μm; C: 20μm.

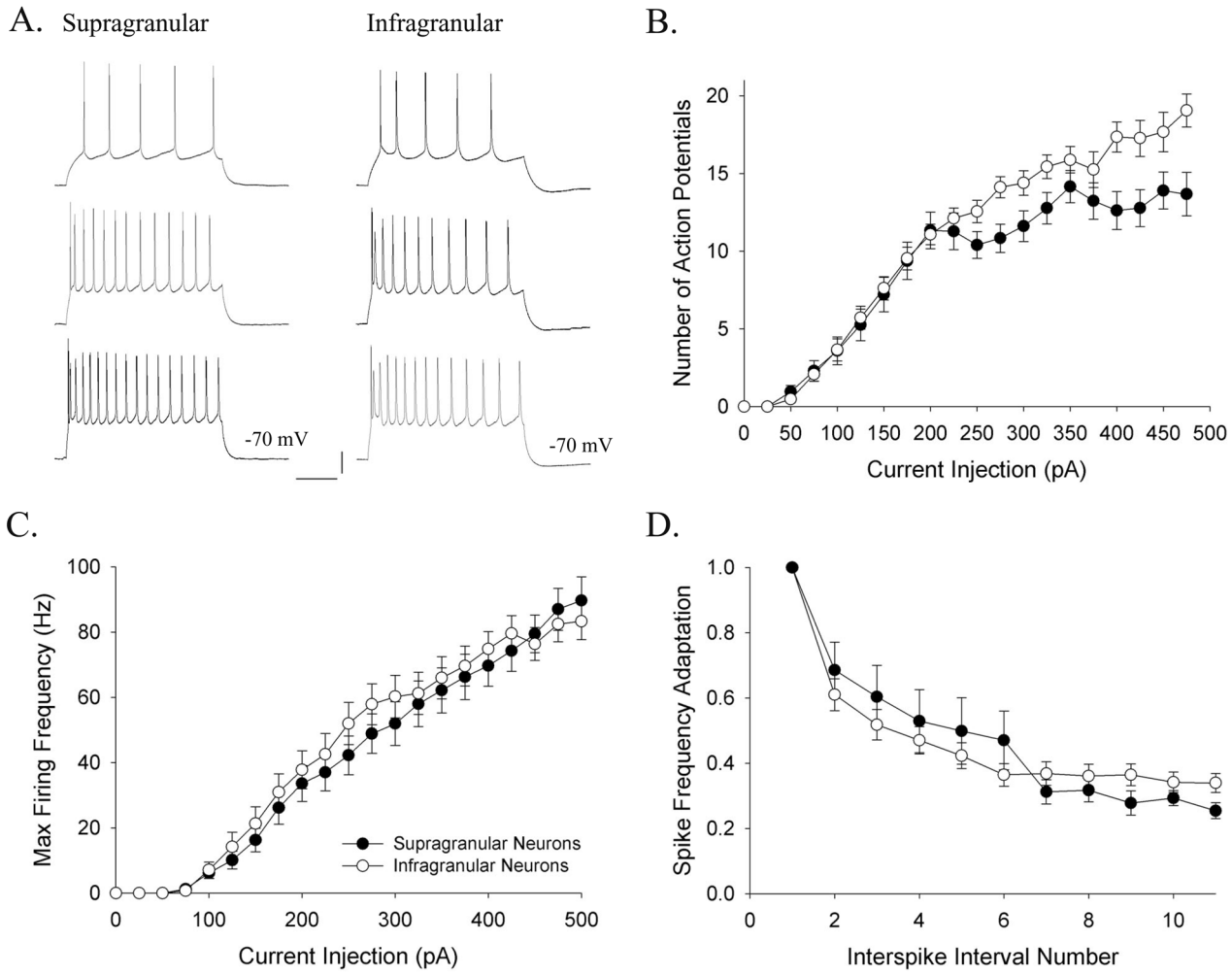

Figure 3.

Response properties of callosal neurons to electrical stimulation. A. Repetitive spiking of supragranular and infragranular callosal neurons to intracellular current injection (in pA: top-100; middle-175; bottom-250). B. Measures of increased spiking and increases in firing frequency (C) of callosal neurons. D. Spike frequency adaptation for current injection measuring 200pA. Calibration in A: 250 ms, 20 mV.

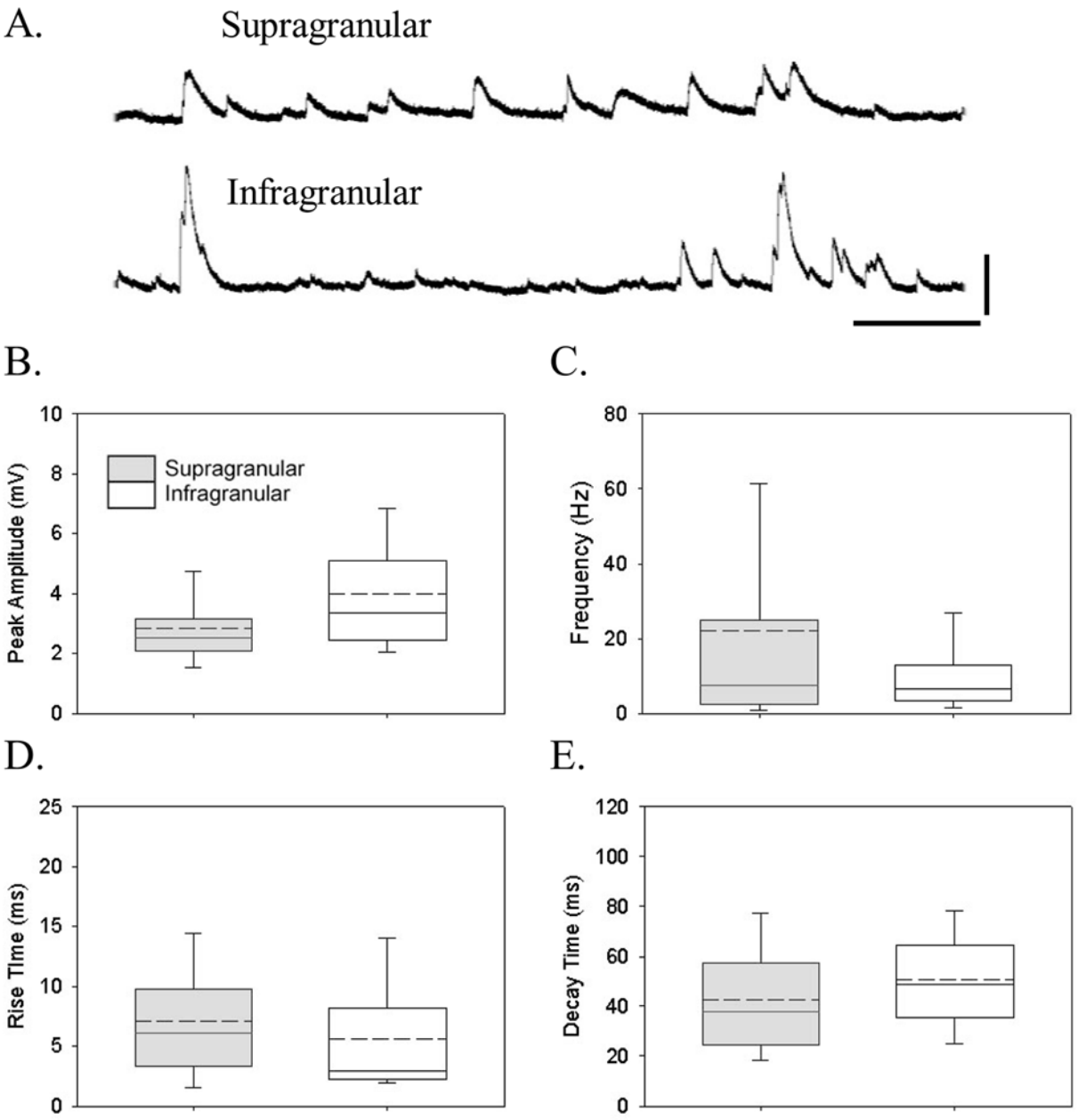

Figure 4.

Spontaneous postsynaptic potentials in SC and IC neurons. A. Representative traces of PSPs in SC (top trace; membrane potential = 78mV) and IC neurons (bottom trace; membrane potential = 77mV) neurons. Comparison of average PSP amplitude (B), frequency (C), rise time (D), and decay time (E) in SC and IC neurons. Calibration in A: 600ms, 5mV.

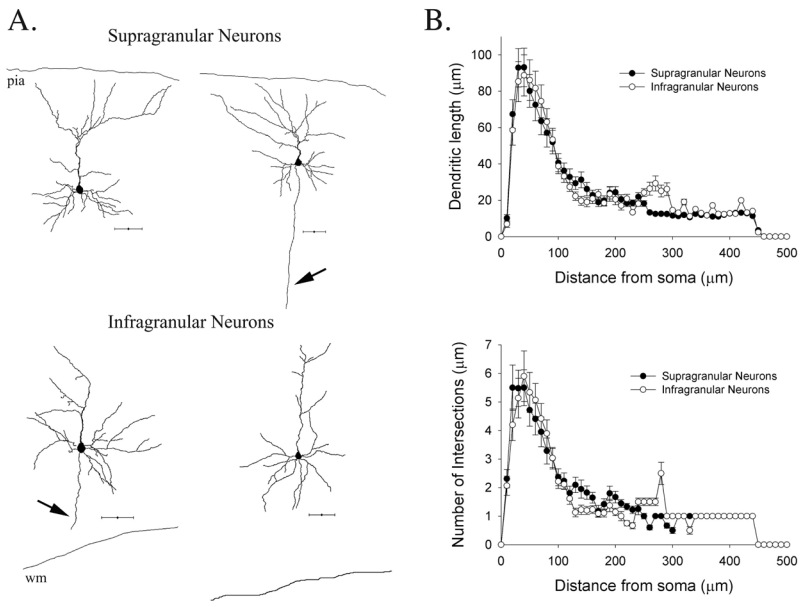

Figure 5.

Morphological reconstruction of biocytin labeled callosal neurons. A. Representative examples of supragranular and infragranular neurons. Arrows point to axons. B. Sholl analysis of dendritic length (top) and number of dendritic intersections (bottom) of reconstructed neurons. Calibration in A: all 50μm.